International Journal of Coal Geology 184 (2017) 57–72

Contents lists available at ScienceDirect

International Journal of Coal Geology

journal homepage: www.elsevier.com/locate/coal

Combined SEM and reflected light petrography of organic matter in the New Albany Shale (Devonian-Mississippian) in the Illinois Basin: A perspective on organic pore development with thermal maturation

Bei Liu[a,*], Juergen Schieber[a], Maria Mastalerz[b]

[a] Department of Earth and Atmospheric Sciences, Indiana University, Bloomington, IN 47405, USA
[b] Indiana Geological and Water Survey, Indiana University, Bloomington, IN 47405-2208, USA

ABSTRACT

Organic-matter-hosted pores are an important aspect of pore systems in unconventional gas shale reservoirs. Along with thermal maturity, organic maceral type critically controls the development of secondary organic-matter-hosted pores. Three New Albany Shale samples (Devonian-Mississippian, kerogen type II sequence) having thermal maturities ranging from a vitrinite reflectance (R_o) of 0.55% to 1.42% were analyzed using a reflected light microscope and a field emission scanning electron microscope. Organic pores were examined in specific organic macerals and solid bitumen at different thermal maturities. Vitrinite and inertinite, derived from terrestrial woody materials, occur as discrete particles in this black shale. Within the resolution limits of the scanning electron microscope, these two macerals do not appear to display enhanced secondary pores associated with increases in thermal maturity. Cellular pores (0.2–10 μm) in inertinite were observed throughout the entire maturity range and were typically filled with authigenic quartz or solid bitumen. Because of thermal degradation, amorphous organic matter was not observed at maturities greater than R_o 0.80%. Alginite derived from *Tasmanites* cysts matures later than amorphous organic matter and is still present at R_o 0.80%; however, it is in the process of transforming to pre-oil bitumen and shows weak orange yellow fluorescence compared to strong greenish-yellow fluorescence in lower-maturity samples. At a maturity of R_o 1.42%, alginite could no longer be observed as a distinct phase because of its complete transformation to hydrocarbons and bitumen. Alginite began to develop secondary pores when it was in the process of transforming to pre-oil bitumen, which indicates that some liquid and gaseous hydrocarbons left the alginite during this part of the maturation process. Solid bitumen developed along the original amorphous organic matter networks and now occupies interparticle space between quartz, dolomite, K-feldspar, clay, and mica grains, as well as the cellular pores in inertinite particles. Solid bitumen becomes smaller and more porous with thermal maturation and, thus, becomes increasingly unidentifiable with the optical microscope. Solid bitumen-hosted pores (20–1000 nm) are the main organic pore type documented in the studied samples, and they are more common in shales within the gas window than those in the oil window. Secondary nanopores in the solid bitumen network play a significant role in hydrocarbon storage and migration.

1. Introduction

Organic-matter-hosted porosity in tight shale reservoirs is significant for hydrocarbon storage and migration (e.g., Wang and Reed, 2009; Slatt and O'Brien, 2011; Hao et al., 2013; Collell et al., 2015). The oil wettability of organic matter (OM) makes organic pores preferential sites for oil and gas storage relative to voids between water-wet mineral grains (Wang and Reed, 2009; Passey et al., 2010). In organic-rich shale gas systems, the gas content of shale reservoirs is positively correlated with total organic carbon (Zuber et al., 2002; Ross and Bustin, 2009; Wang and Reed, 2009; Strąpoć et al., 2010; Xue et al., 2016), and up to half of the methane can be stored in organic matter as adsorbed gas (Fan et al., 2014).

Organic pores are normally thought to form when oil and gas are generated and expelled (Loucks et al., 2009; Wang and Reed, 2009; Bernard et al., 2012). To date, all observed OM-hosted nanopores (< 1000 nm) were documented with scanning electron microscope (SEM) or transmission electron microscope (TEM) (Loucks et al., 2009; Ambrose et al., 2010; Schieber, 2010; Sondergeld et al., 2010; Curtis et al., 2011; Chalmers et al., 2012; Loucks et al., 2012; Milliken et al.,

* Corresponding author.
E-mail address: liubei@umail.iu.edu (B. Liu).

https://doi.org/10.1016/j.coal.2017.11.002
Received 5 July 2017; Received in revised form 30 October 2017; Accepted 1 November 2017

2013). Other techniques, such as gas adsorption and molecular simulation, also support the presence of micropores (< 2 nm) in the macromolecular structure of OM. Rexer et al. (2014) measured the micropore volume and specific surface area of isolated kerogens of the Posidonia Shale (Jurassic) of northern Germany using low-pressure CO_2 and N_2 adsorption and found that micropore volume and specific surface area of OM increase with thermal maturity. Bousige et al. (2016) modeled the molecular structure of kerogen and derived the micropore structure and specific surface area of kerogens; they concluded that the specific surface area of kerogens increases with thermal maturity. Secondary organic pores have been observed in both gas-window-maturity shales (Bernard et al., 2012; Curtis et al., 2012) and oil-window-maturity shales (Loucks and Reed, 2014; Reed et al., 2014). Some studies, however, suggest that organic porosity is not restricted to thermally mature shales. Fishman et al. (2012) studied organic pores in the Kimmeridge Clay Formation (Jurassic) of the North Sea and concluded that organic pores were not related to thermogenic hydrocarbon generation, based on similar pore size and shape in thermally immature and mature samples. The authors suggest that organic pores in thermally immature samples could be attributed to methanogenesis or predepositional transformational processes of OM and that secondary organic pores in clay-rich shales tend to collapse because of compaction. Löhr et al. (2015) suggested that thermally immature OM can host organic pores, which have an impact on the development of secondary OM-hosted pores by providing space for pore-filling bitumen, particularly in structured organic matter.

In some high-maturity organic-rich shales, some OM particles have very well-developed secondary porosity, whereas other OM particles in the same sample show no porosity at SEM resolution (Loucks et al., 2009; Curtis et al., 2012; Milliken et al., 2013). This prompted Schieber (2010) to suggest that the structural state of OM (e.g., the degree of polymerization) is another important control on the development of organic porosity. Misch et al. (2016) reported that primary macerals (vitrinite and inertinite) do not develop SEM-visible secondary pores even at dry gas window maturity levels. Bernard et al. (2012) concluded that secondary OM nanopores exist only in pyrobitumen in gas-window-maturity shales. In contrast, Reed et al. (2014) reported that solid bitumen (SB) in oil-window-maturity shales can also host OM pores. A likely cause for these contradictory findings is the fact that the differentiation of organic macerals is difficult to impossible using electron microscopy, although under fortunate circumstances, depositional (kerogen) and migrated OM (SB) can be distinguished under SEM, based on morphology and contact with minerals (Loucks and Reed, 2014; Milliken et al., 2014). Hackley et al. (2017) used integrated correlative light and electron microscopy to image sedimentary OM in shales and differentiated nonfluorescent SB and fluorescent amorphous organic matter (AOM) successfully, but correlative fluorescence and electron microscopy is applicable only to samples having thermal maturities of up to about 1.0 to 1.1% R_o.

The focus of this investigation is to study the evolution of secondary pores in specific organic macerals and SB in relation to the level of thermal maturation. Specific objectives are: (1) to identify organic macerals (AOM, alginite, vitrinite, inertinite) and SB in the New Albany Shale at various thermal maturities using a reflected light microscope; and (2) document via SEM the level and style of secondary pore development in the exact same OM particles.

2. Methods and materials

SEM observations of ion-milled samples allow us to image nanometer-scale pores in OM in shale reservoirs. However, organic matter is invariably black under the SEM regardless of the electron imaging mode. It is, therefore, very difficult if not impossible to distinguish them (Camp, 2016b; Valentine and Hackley, 2016; Hackley et al., 2017). In contrast, identifying organic maceral using the optical microscope under reflected light and oil immersion is routinely used in organic petrography of coal and shale (Taylor et al., 1998; Hackley and Cardott, 2016). Particle-specific application of both SEM and organic petrography should, therefore, allow us to observe pores in specific OM particles.

The New Albany Shale of the Illinois Basin is a Middle Devonian to Lower Mississippian organic-rich formation with the main deposition in the Late Devonian (Lineback, 1964, 1968; Cluff, 1980; Beier and Hayes, 1989; Ripley et al., 1990; Lazar, 2007; Strąpoć et al., 2010). This formation is interpreted to have been deposited in an epicontinental sea (Lineback, 1968; Cluff, 1980; Beier and Hayes, 1989; Ripley et al., 1990; Lazar, 2007). The New Albany Shale is composed of black laminated shales and greenish-gray bioturbated shales with interbedded siltstone, sandstone, limestone, and dolostone of limited extent and thickness (Lineback, 1964, 1968; Cluff, 1980; Beier and Hayes, 1989; Lazar, 2007). It extends from central and southern Illinois to southwestern Indiana and western Kentucky with a thickness from < 6 to 140 m and vitrinite reflectance (R_o) from 0.5% near the basin margin to 1.5% in the deepest part of the basin (Strąpoć et al., 2010; Mastalerz et al., 2013). Organic matter in the New Albany Shale is classified as type II kerogen based on pyrolysis analysis (Chou et al., 1991).

For this study, we selected three New Albany Shale samples that cover a range of thermal maturity from R_o 0.55% to 1.42%. An early mature sample (R_o 0.55%), an oil-window-maturity sample (R_o 0.80%), and a gas-window-maturity sample (R_o 1.42%) were from Daviess County, Indiana, Webster County, Kentucky, and Hicks Dome, Illinois, respectively (Fig. 1). The early mature and oil-window-maturity samples are from drill cores, and the gas-window-maturity sample is an outcrop sample. All samples are from the core library of the Indiana Geological and Water Survey. Only megascopically homogeneous black shales having a high total organic carbon (TOC) content were selected. Other factors, such as depositional environment, mineral composition, and rock mechanical properties were not considered. The early mature sample is a combination of dolomitic and siliceous shale and the oil-window- and gas-window-maturity samples are siliceous shales based on SEM observations.

The TOC content of shale samples was measured using a Leco analyzer (SC832DR). The method of measuring total pore volume and porosity has been described in Mastalerz et al. (2013).

Shale samples of each maturity were crushed to rock chips of < 2 mm to make two whole-rock pellets. One pellet having a large amount of rock chips was used for measuring vitrinite reflectance and organic petrographic composition; one pellet containing only three rock chips was used for petrographic observation under reflected light microscope and SEM.

The R_o of the shale samples was measured on mechanically polished whole-rock pellets under reflected white light and oil immersion with 50 measurements. We determined the quantitative organic petrographic composition of the shale samples using a point-counting method with 500 points counted only on OM, based on the ICCP (1998, 2001) classification and Pickel et al. (2017). The maceral groups vitrinite and inertinite were not classified into macerals because of their scarcity. Only the major macerals including AOM (bituminite), alginite, and liptodetrinite were considered for liptinite. Solid bitumen was included in the measurement of organic petrographic composition because of its increasing content with thermal maturity.

Organic macerals including vitrinite, inertinite, amorphous organic matter, alginite and SB in the whole-rock pellets with three rock chips were identified using a reflected light microscope (Leica DFC310 FX) and photographed/mapped to enable the subsequent relocation of the same OM particles under SEM. Then the whole-rock pellets were cut to remove the lucite from the three rock chips and the surfaces examined by organic petrography were argon-ion-milled with a Gatan 600 DuoMill using a custom-designed sample holder at a low incident angle and 4 kV for 1 h (Schieber, 2010, 2013; Schieber et al., 2016). The ion-milled surfaces were then examined without a conductive coating using a field emission SEM (FEI Quanta 400 FEG) in low vacuum mode. The

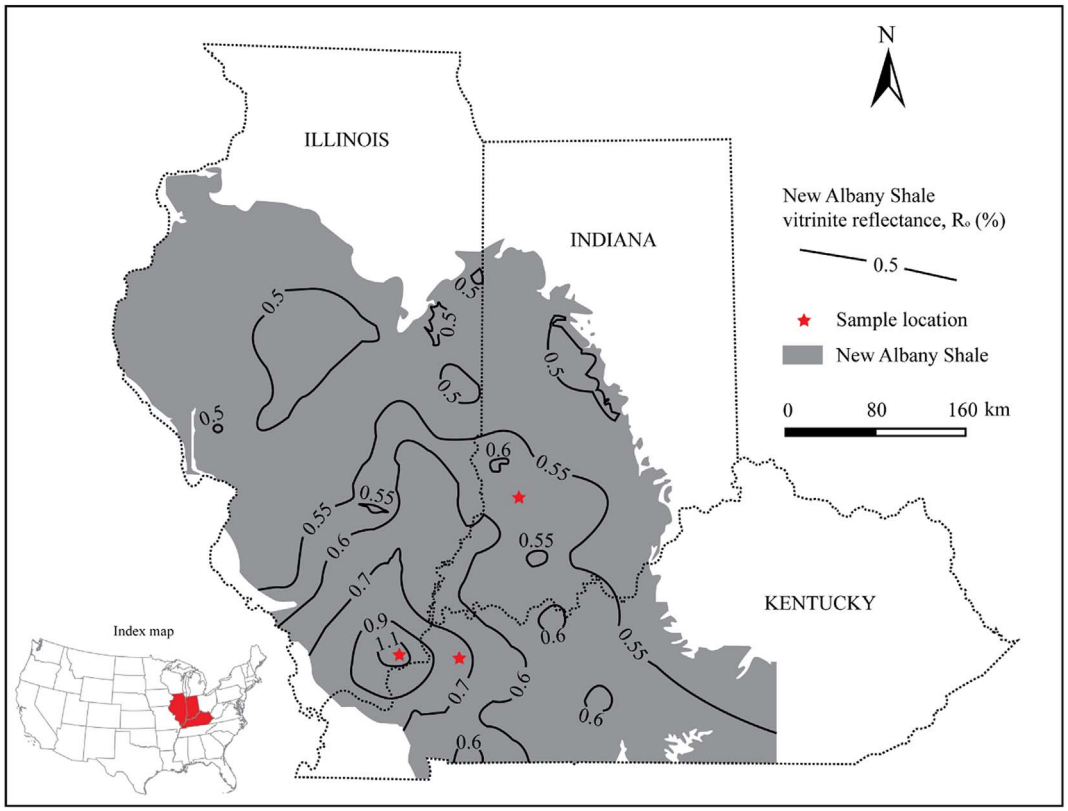

Fig. 1. Map showing the locations of sampling sites and the vitrinite reflectance contour lines of the New Albany Shale. Modified from Mastalerz et al. (2013).

working distance was about 10 mm, and the accelerating voltage was 15 kV. A large-field detector was used for detecting secondary electrons in low vacuum mode. The morphology and pore development of OM particles were documented at each thermal maturity. All SEM pictures were taken under secondary electron imaging mode. Schematic diagrams of a typical SEM and a reflected light microscope can be found at Sutton et al. (2007) and Ganser and Weiss (2008), respectively. Correlative microscopy was conducted on two sets of samples in this study to take into account limitations imposed by the heterogeneity of shales (e.g., rareness of vitrinite, different generations of SB, etc.).

3. Results

3.1. Organic petrology and porosity

The TOC content decreases from 10.77 wt% in the early mature sample (R_o 0.55%) to 4.26 wt% in the oil-window-maturity sample (R_o 0.80%) and 2.58 wt% in the gas-window-maturity sample (R_o 1.42%, Table 1), which to some degree parallels the loss of organic matter when oil-prone kerogens are transformed to hydrocarbons. However, the difference between the TOC contents of these samples may not actually reflect the loss of organic carbon during thermal maturation, because the original TOC contents of oil-window-maturity and gas-window-maturity samples are unknown.

Amorphous organic matter (bituminite) is the dominant organic component in the early mature sample (R_o 0.55%), accounting for 64.87% of total OM (Table 1; Fig. 2). Alginite (18.96%) is second to AOM. Only 3.35% of the OM is SB at this maturity, which might be a result of early transformation of labile kerogen. In the oil-window-maturity sample (R_o 0.80%), SB becomes the dominant OM, accounting for 68.09% of total OM. The proportion of alginite (16.54%) does not change significantly. Amorphous organic matter was not observed at this maturity, suggesting that it has undergone complete degradation to hydrocarbons and bitumen at this point in thermal evolution. Solid bitumen (97.17%) is the dominant OM in the gas-window-maturity sample (R_o 1.42%), because oil-prone kerogens (AOM and alginite) have been transformed to hydrocarbons and bitumen. Vitrinite and inertinite derived from terrestrial higher plants are present in minor amounts in all samples (Table 1; Fig. 2).

Table 1
Vitrinite reflectance (R_o), total organic carbon (TOC) content, maturity stage, and organic petrographic composition of shale samples (modified from Mastalerz et al., 2013).

Sample	R_o (%)	TOC (wt %)	Maturity stage	Organic petrographic composition (volume %, on mineral-matter-free basis)					
				AOM	AL	LPD	SB	I	V
Dav	0.55	10.77	Early mature	64.87	18.96	4.65	3.35	7.43	0.74
Web	0.80	4.26	Middle mature		16.54	2.33	68.09	12.45	0.58
IL-3	1.42	2.58	Post mature				97.17	2.26	0.57

AOM = amorphous organic matter; AL = alginite; LPD = liptodetrinite; SB = solid bitumen; I = inertinite; V = vitrinite.

The grain density of the shale samples increases with increasing thermal maturity (Table 2), which may result from the loss of OM with the thermal evolution of OM. There is a slight increase in total porosity of the studied samples with increasing thermal maturity, especially from the oil-window-maturity to gas-window-maturity sample (Table 2). A potential explanation for this is that secondary organic pores develop during thermal maturation, although other factors such as mineralogical composition and diagenesis (e.g., carbonate dissolution) also influence porosity.

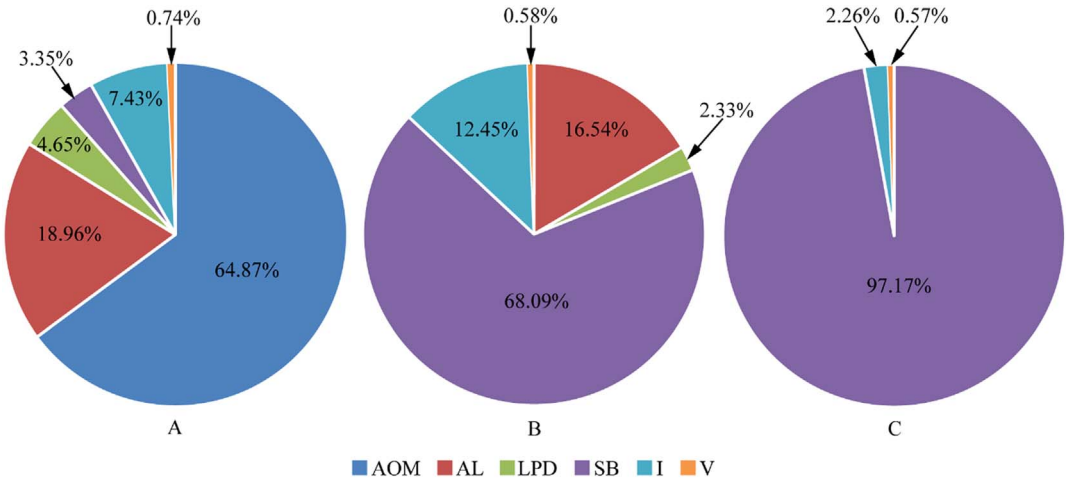

Fig. 2. Pie charts illustrating the organic petrographic compositions of shale samples. (A) Early mature sample (R_o 0.55%); (B) Oil-window-maturity sample (R_o 0.80%); (C) Gas-window-maturity sample (R_o 1.42%).

Table 2
Porosity of shale samples based on helium porosimetry.

Sample	R_o (%)	Grain density (g/cm^3)	Bulk density (g/cm^3)	Total pore volume (cm^3/g)	Total porosity (%)
Dav	0.55	2.14	2.06	0.0181	3.74
Web	0.80	2.22	2.13	0.0190	4.05
IL-3	1.42	2.43	2.30	0.0233	5.35

3.2. Early mature sample

Vitrinite and inertinite (derived from terrestrial vegetation) occur as discrete particles in the mineral matrix (Fig. 3A–F). Because they were transported to the marine environment from the continent, they likely experienced some sorting and rounding in the process. No pores were observed in vitrinite and in most inertinite (Fig. 3B, D) at SEM resolution. Cellular pores were observed in inertinite (Fig. 3F). In this study, cellular pores in inertinite range from 0.2 to 10 μm (Fig. 3F) and are typically filled with authigenic quartz (Fig. 3F).

Alginite is represented by elongated algal bodies (compacted *Tasmanites* cysts) admixed with AOM (Fig. 3G–J). Alginite at this maturity shows strong greenish-yellow fluorescence (Fig. 3H) and is frequently associated with authigenic minerals such as pyrite (Fig. 3I). No SEM-visible pores were observed in alginite (Fig. 3J).

Amorphous organic matter occurs as organic streaks parallel to the bedding plane (Fig. 3E, I, K). These organic streaks commonly touch each other and form an organic network in black shale of this maturity. No pores were observed in AOM (Fig. 3L) at SEM resolution.

Solid bitumen occupies interparticle space (Figs. 3I–J, 4A–B) and cavity space (Fig. 4C–D). The transition from AOM to SB (Fig. 4E–F) that is observed in places indicates that an SB network had started to replace the original AOM network. It also demonstrates that SEM cannot distinguish OM type (Fig. 4E–F). The size of SB areas is commonly larger than 50 μm at this maturity (Fig. 4A–B).

3.3. Oil-window-maturity sample

As in the early mature sample, vitrinite and inertinite are present as discrete particles (Fig. 5A–F). Vitrinite and inertinite do not show secondary pores under SEM (Fig. 5B, D). Cellular pores in inertinite could still be observed, and they are typically filled with authigenic quartz (Fig. 5F).

Alginite, in contrast, is no longer present simply as flattened *Tasmanites* cysts. Most of the alginite experienced thermal degradation and occurs now as clumps of OM (Fig. 5G–H). Under the optical microscope, alginite is dark in reflected light (Fig. 5G) and shows weak orange yellow fluorescence (Fig. 5H). The newly formed pre-oil bitumen is totally black (Fig. 5I) and shows no fluorescence (Fig. 5J), which indicates that the former alginite has undergone complete transformation to pre-oil bitumen. Alginite in places shows flow characteristics (Fig. 5K–L) and secondary pores development at this maturity (Fig. 5M–N). The porous area in alginite appears to be associated with minerals, which may be explained by the catalytic reaction of minerals in the thermal degradation process of OM.

The occurrence of SB is the same as that in the early mature sample, which occupies interparticle space (Fig. 6A–F) and cavity space (Fig. 6G–H). Large pieces of SB (> 50 μm) are connected with small particles of SB (< 1 μm) (Fig. 6A–B). Solid bitumen is the dominant OM at this maturity and forms an organic network in the studied samples. Secondary organic pores were observed in small particles of SB (Fig. 6D–F). The shape of pores in SB can be round or irregular. Interestingly, large pieces of SB do not show organic pores (Fig. 6B). Small particles of SB with secondary nanopores (< 1000 nm) are at the limit of resolution of reflected light microscopy (Fig. 6C–E). Solid bitumen filling cellular pores in inertinite is generally porous (Fig. 6H).

3.4. Gas-window-maturity sample

Similar to previous samples, vitrinite and inertinite are present as discrete particles in the mineral matrix (Fig. 7A–F). Vitrinite and inertinite do not show secondary pores (Fig. 7B, D). Cellular pores in inertinite are still very common and they are typically filled with authigenic quartz (Fig. 7F). Detrital particles (e.g., clay-sized minerals or organic debris) can fill cellular pores as well (Fig. 7F).

Solid bitumen is the dominant OM at the maturity of R_o 1.42%. Solid bitumen occupies interparticle space (Fig. 8A–H) and cavity space (Fig. 8I–J). Large pieces of SB (> 50 μm), such as those present in the lower-maturity samples, were not observed, and most SB particles are < 20 μm in size. Similar to the oil-window-maturity sample, SB with well-developed secondary nanopores was almost unidentifiable at the resolution of an optical microscope (Fig. 8A–D).

More secondary nanopores were observed in SB at this maturity than in the oil-window-maturity sample (Fig. 8B, D–F) based on visual estimate. Solid bitumen-hosted nanopores can be round or irregular in shape, which is very similar to the SB-hosted pores in the oil-window-maturity sample. The size of secondary pores in SB ranges from 20 to 1000 nm (Fig. 8B, D–F). However, there are cases where pore-filling SB that occurs adjacent to porous SB does not show secondary pore development (Fig. 8H). Solid bitumen that fills cellular pores in inertinite

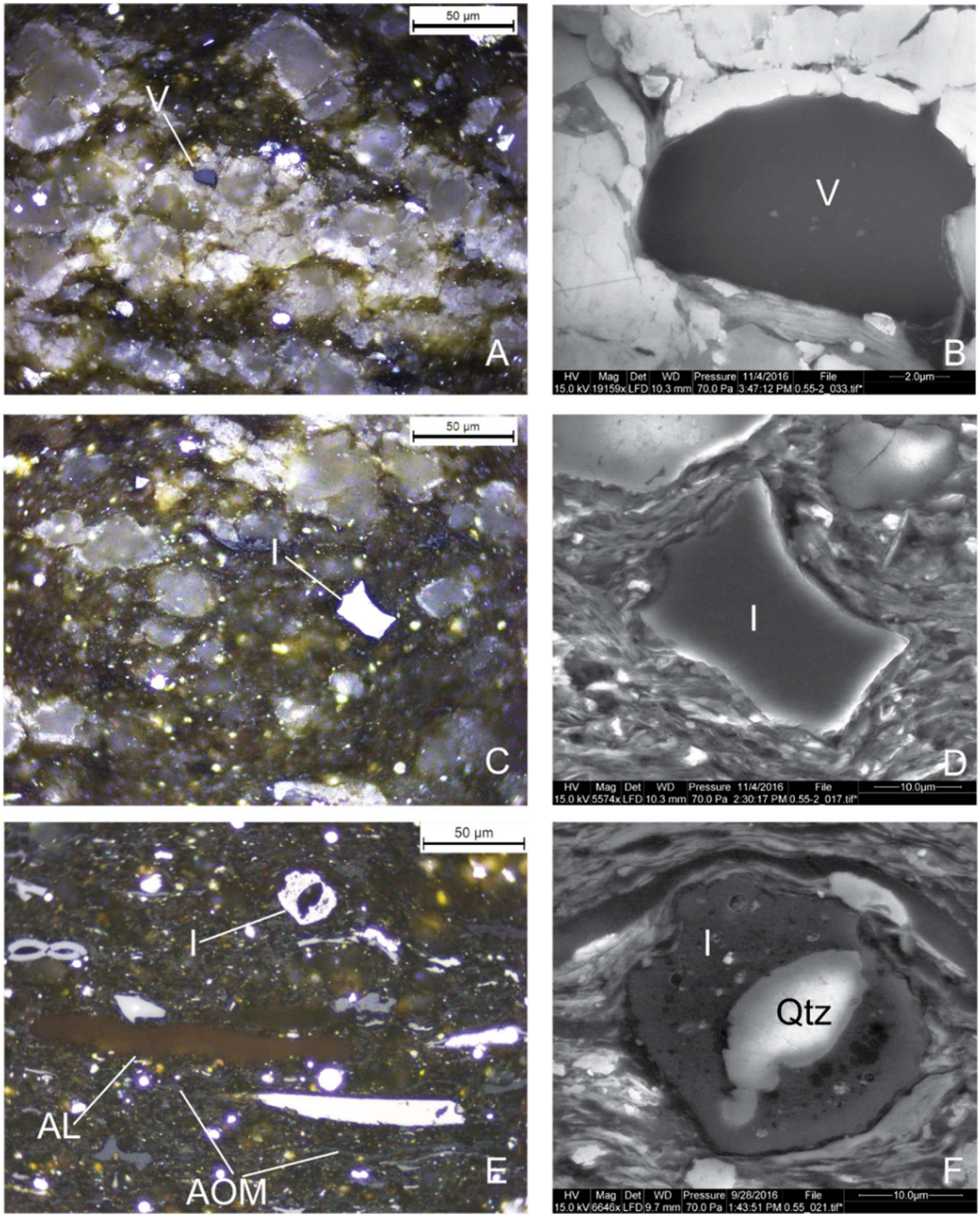

Fig. 3. Photomicrographs of primary organic matter under reflected light and oil immersion (A, C, E, G, I, K), blue fluorescent light (H), and their correlative SEM images (B, D, F, J, L, secondary electron images) in the early mature sample, R_o 0.55%. (A) Vitrinite; (B) SEM image of vitrinite in A; (C) Inertinite without cellular pores; (D) SEM image of inertinite in C; (E) Inertinite with cellular pores; (F) SEM image of inertinite in E. The cellular pores are filled with authigenic quartz; (G) Alginite derived from *Tasmanites* cysts; (H) Alginite in G under blue fluorescent light; (I) Alginite filled with authigenic pyrite; (J) SEM image of alignite in I; (K) Amorphous organic matter; (L) SEM image of the red dotted framed area in K. V = vitrinite; I = inertinite; AOM = amorphous organic matter; AL = alginite; SB = solid bitumen; Qtz = quartz; Py = pyrite.

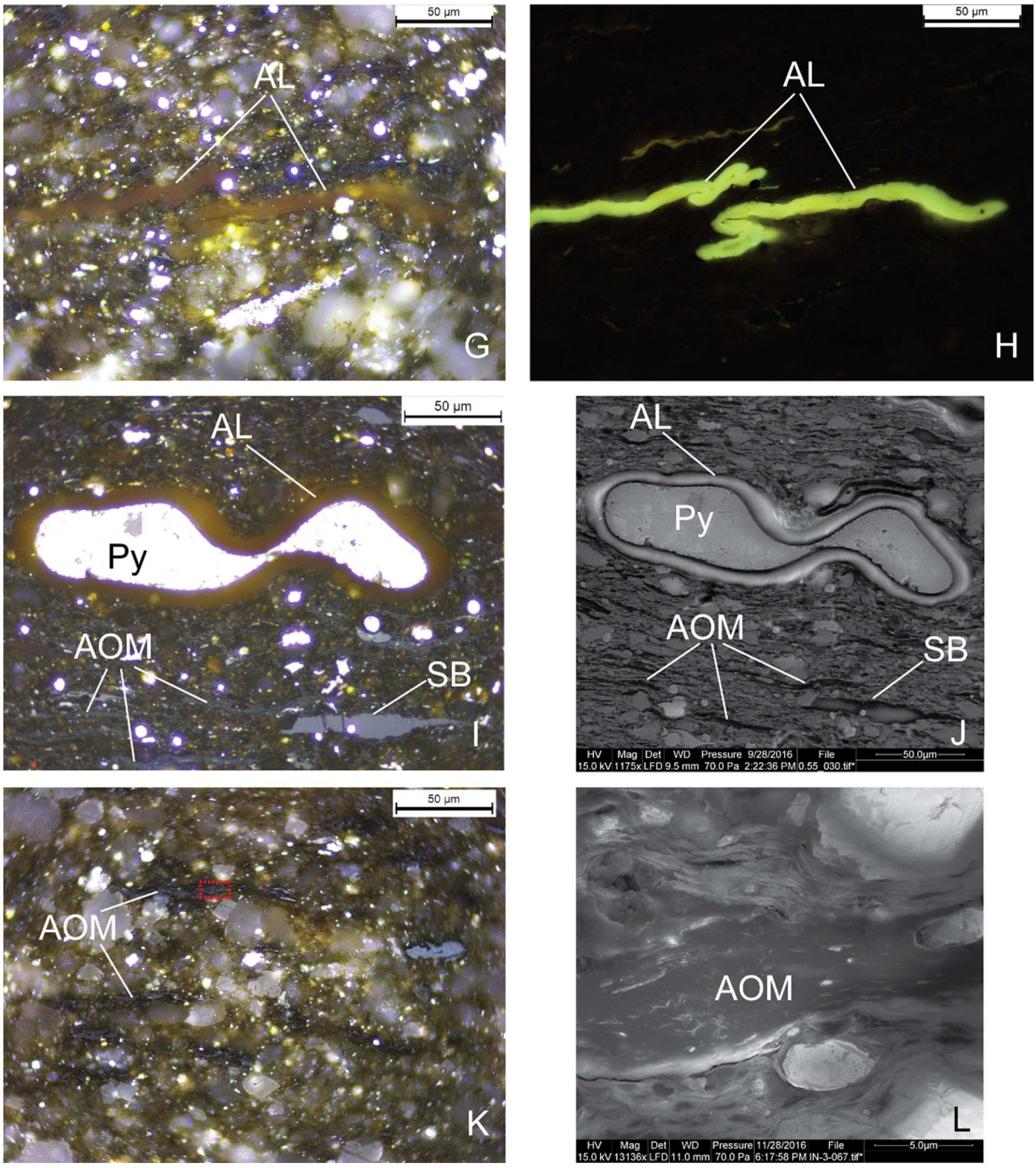

Fig. 3. (*continued*)

is commonly porous (Fig. 8J).

4. Discussion

4.1. Transformation of organic macerals during thermal maturation

Amorphous organic matter, alginite, vitrinite and inertinite are primary OM (kerogen) that was deposited at the same time as the mineral matrix, whereas SB is secondary OM formed through thermal degradation of oil-prone kerogens (Curiale, 1986; Jacob, 1989). The term "solid bitumen" used by organic petrographers differs from what organic geochemists call bitumen. The organic geochemical definition of bitumen is the organic component that can be removed by typical organic solvents (Vandenbroucke and Largeau, 2007; Hackley and Cardott, 2016). Solid bitumen can be differentiated from pyrobitumen under SEM based on the existence of devolatilization cracks (Loucks and Reed, 2014). In this study, SB refers to secondary organic matter that includes pre-oil bitumen, post-oil bitumen, and pyrobitumen used in other studies (Curiale, 1986; Bernard et al., 2012; Loucks and Reed, 2014).

Amorphous organic matter (type II kerogen in the New Albany Shale) could not be identified under an optical microscope (reflected white light and oil immersion) at a maturity of R_o 0.80%, and alginite derived from *Tasmanites* cysts could not be identified at R_o 1.42%. Other studies suggest that the transformation ratio (TR) of type II kerogen approaches up to 50% at a maturity of R_o 0.80%, but the TR of type I kerogen is < 10% at this maturity level (Waples and Marzi, 1998), which could explain the absence of AOM and transformation of

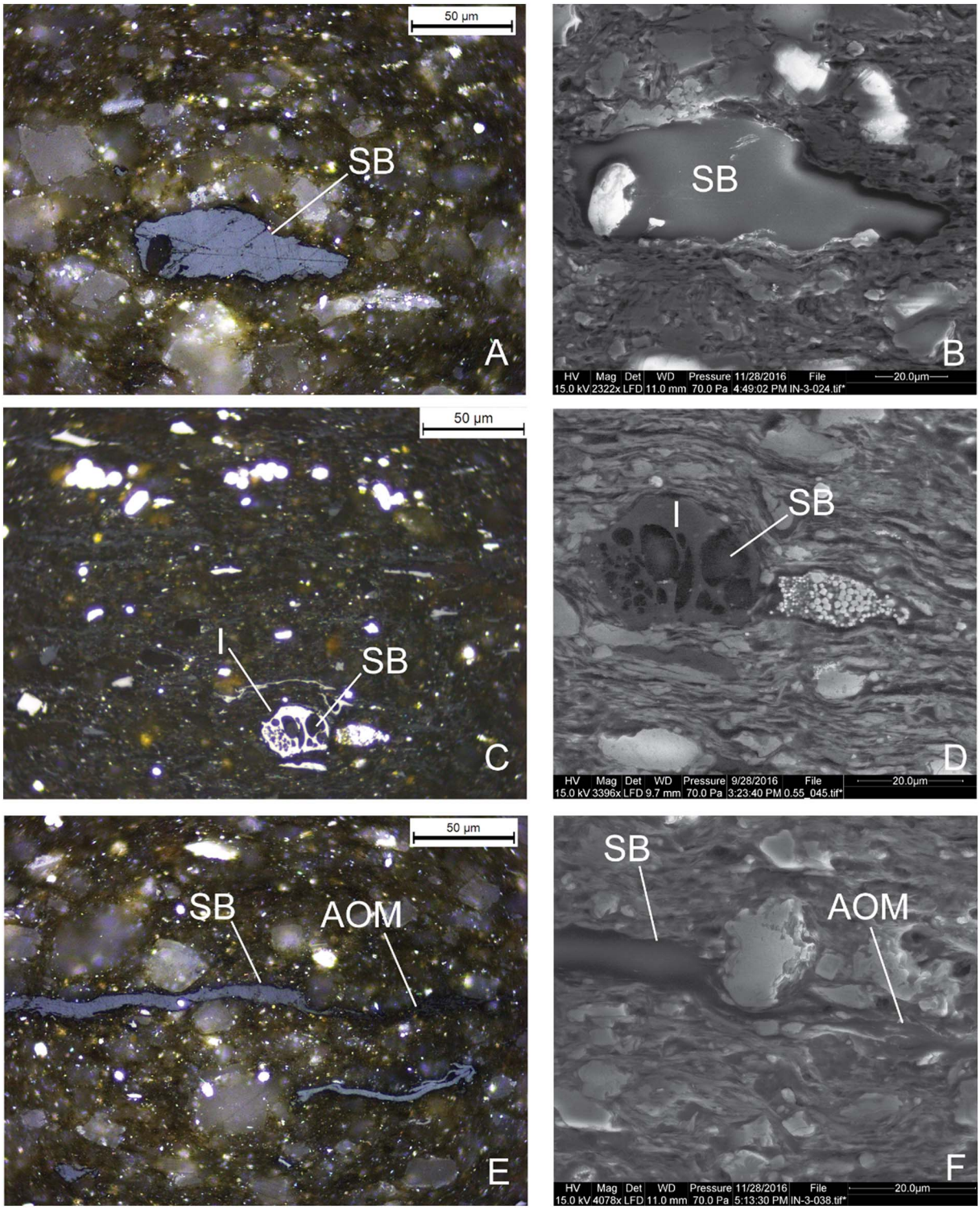

Fig. 4. Photomicrographs of solid bitumen (SB) under reflected light and oil immersion (A, C, E), and their correlative SEM images (B, D, F, secondary electron images) in the early mature sample, R_o 0.55%. (A) Solid bitumen; (B) SEM image of SB in A; (C) SB filling cellular pores in inertinite; (D) SEM image of inertinite and SB in C. (E) SB associated with AOM; (F) SEM image of SB and AOM in E. I = inertinite; AOM = amorphous organic matter; SB = solid bitumen.

alginite to pre-oil bitumen at this maturity. Vigran et al. (2008) reported that alginite derived from *Tasmanites* cysts (type I kerogen) requires a higher temperature to generate hydrocarbons than type II kerogen in the Middle Triassic source rocks of Svalbard and the Barents Shelf. At a maturity of R_o 1.42%, the TR of both AOM and alginite exceeds 90% (Waples and Marzi, 1998), which could explain the absence of alginite at this maturity. Because at R_o 0.80%, alginite represented by *Tasmanites* cysts was already markedly transformed, it likely achieved its complete transformation to hydrocarbons and bitumen well before R_o 1.42%. Hackley and Cardott (2016) suggested that SB is the dominant organic matter in black shales at the peak oil window maturity (R_o ~ 0.9–1.1%) because oil-prone kerogen type I/II is converted to hydrocarbons.

In comparison to alginite and AOM, vitrinite and inertinite (kerogen

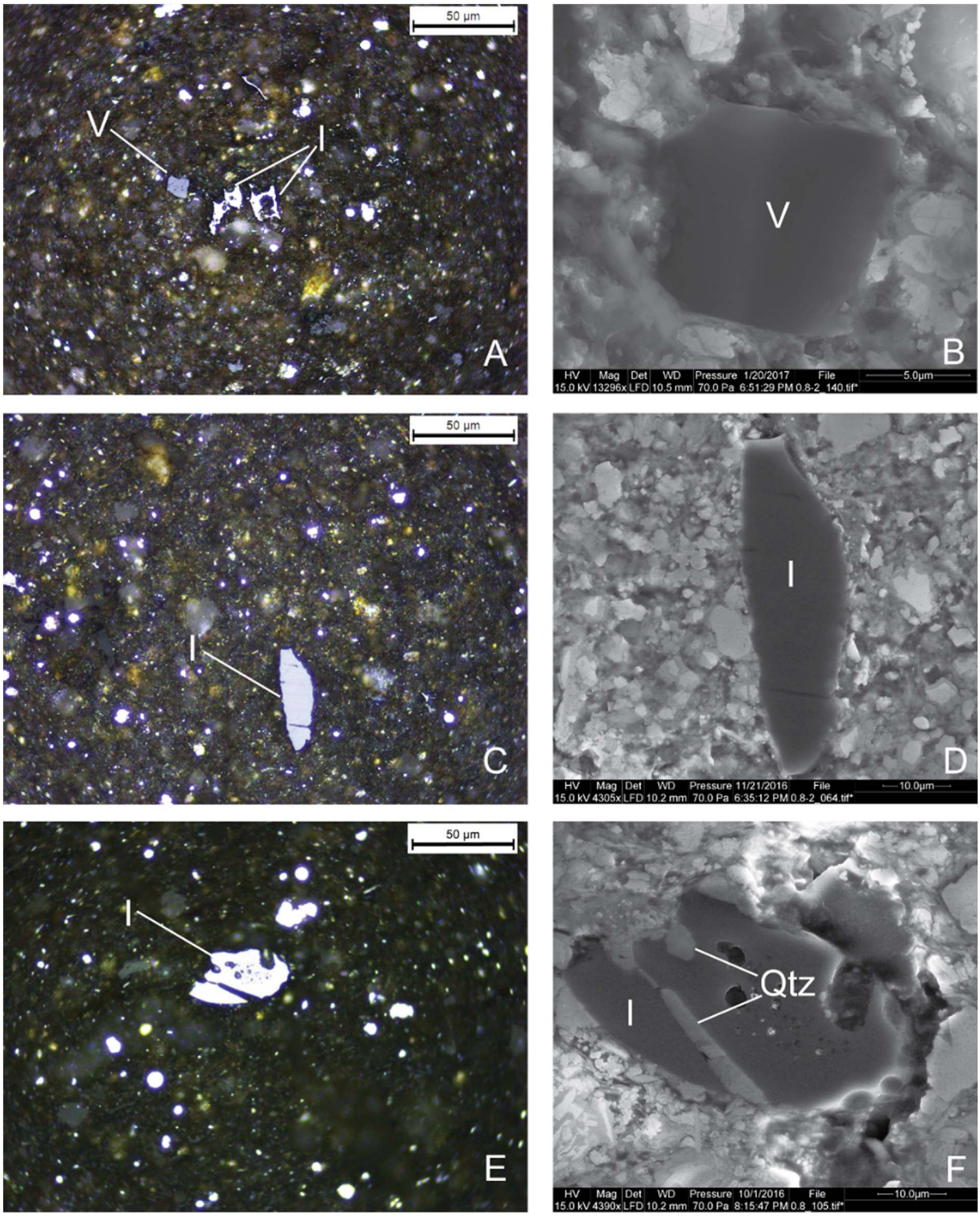

Fig. 5. Photomicrographs of primary organic matter under reflected light and oil immersion (A, C, E, G, I, K), blue fluorescent light (H, J), and their correlative SEM images (B, D, F, L–N, secondary electron images) in the oil-window-maturity sample, R_o 0.80%. (A) Vitrinite; (B) SEM image of vitrinite in A; (C) Inertinite without cellular pores; (D) SEM image of inertinite in C; (E) Inertinite with cellular pores; (F) SEM image of inertinite in E. The cellular pores are filled with authigenic quartz; (G) Alginite; (H) Alginite in G under blue fluorescent light; (I) Pre-oil bitumen transformed from alginite; (J) Pre-oil bitumen in I under blue fluorescent light; (K) Alginite; (L) SEM image of alginite in K; (M) SEM image of the red dotted framed area in L; (N) SEM image of the red dotted framed area in M. Secondary pores in bitumen converted from alginite. V = vitrinite; I = inertinite; AL = alginite; Qtz = quartz; Dol = dolomite.

type III and IV) derived from terrestrial woody materials do not have a high hydrocarbon generation potential, so they do not show significant change in morphology with increasing thermal maturity. Vitrinite and inertinite are present as distinct particles across the entire maturity range (Figs. 3A–F, 5A–F, 7A–F).

4.2. Occurrence of solid bitumen

Oil-prone kerogen is first transformed to pre-oil bitumen and then to oil, gas, and post-oil bitumen or pyrobitumen during thermal maturation (Jarvie et al., 2007; Loucks and Reed, 2014; Camp, 2016a). In the

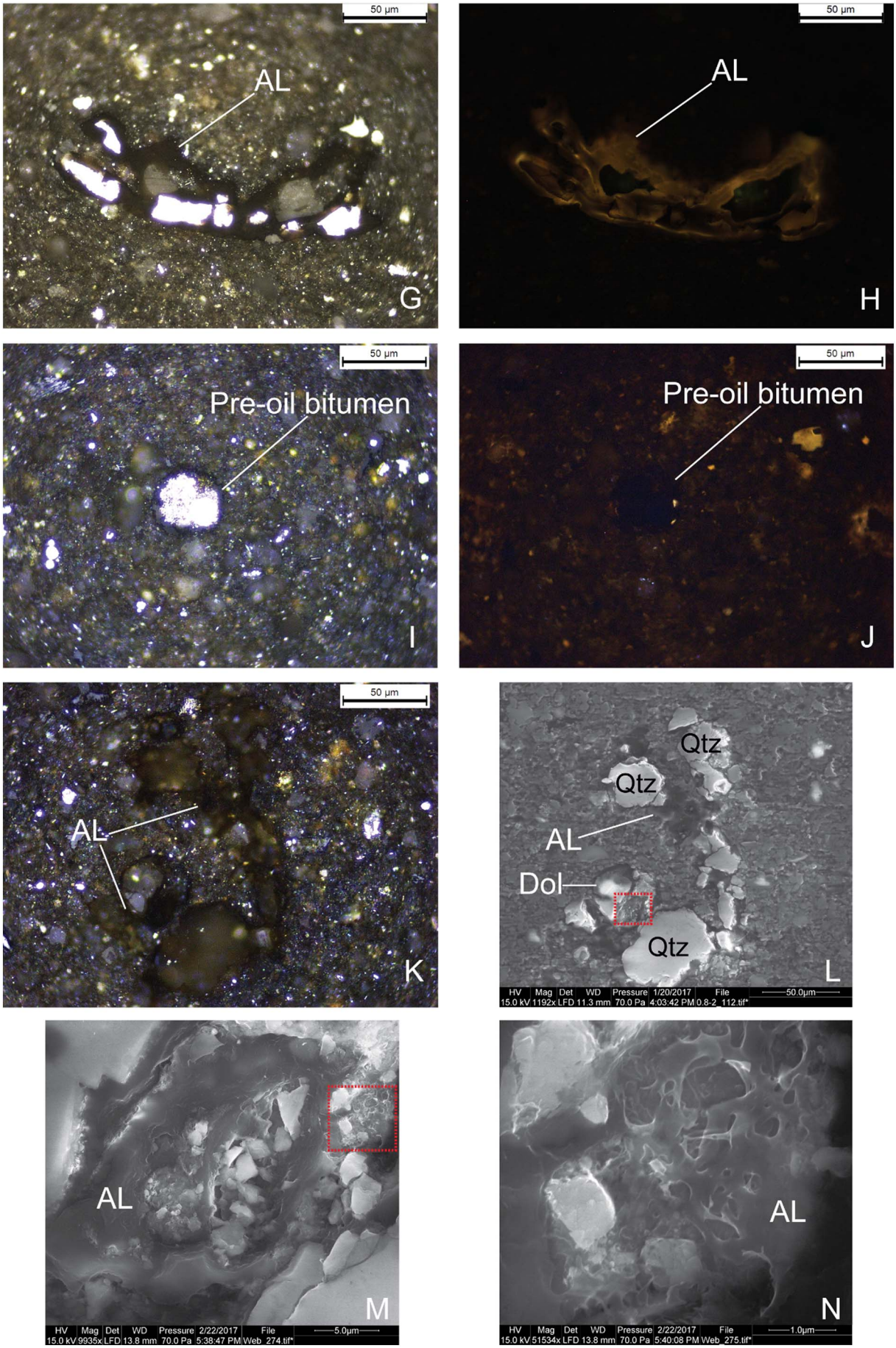

Fig. 5. (*continued*)

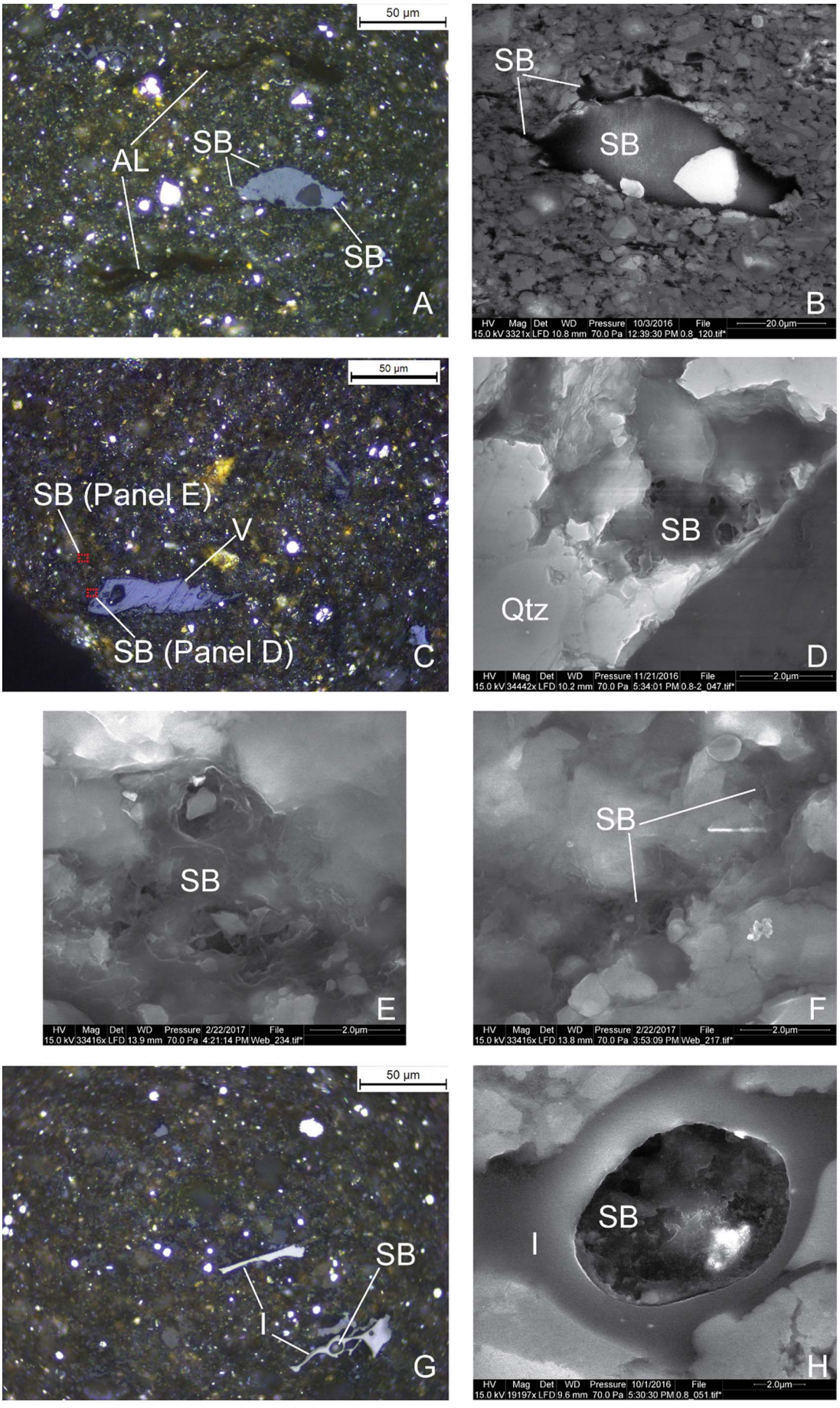

(caption on next page)

Fig. 6. Photomicrographs of solid bitumen (SB) under reflected light and oil immersion (A, C, G), and their correlative SEM images (B, D–F, H, secondary electron images) in the oil-window-maturity sample, R_o 0.80%. (A) A large piece of SB interconnected with small particles of SB; (B) SEM image of SB in A; (C) Small particles of SB filling pore space between mineral grains; (D–F) SEM images of small particles of SB with secondary nanopores; (G) SB filling cellular pores in inertinite; (H) SEM image of inertinite and SB in G. This SB shows secondary nanopores. V = vitrinite; I = inertinite; AL = alginite; SB = solid bitumen; Qtz = quartz.

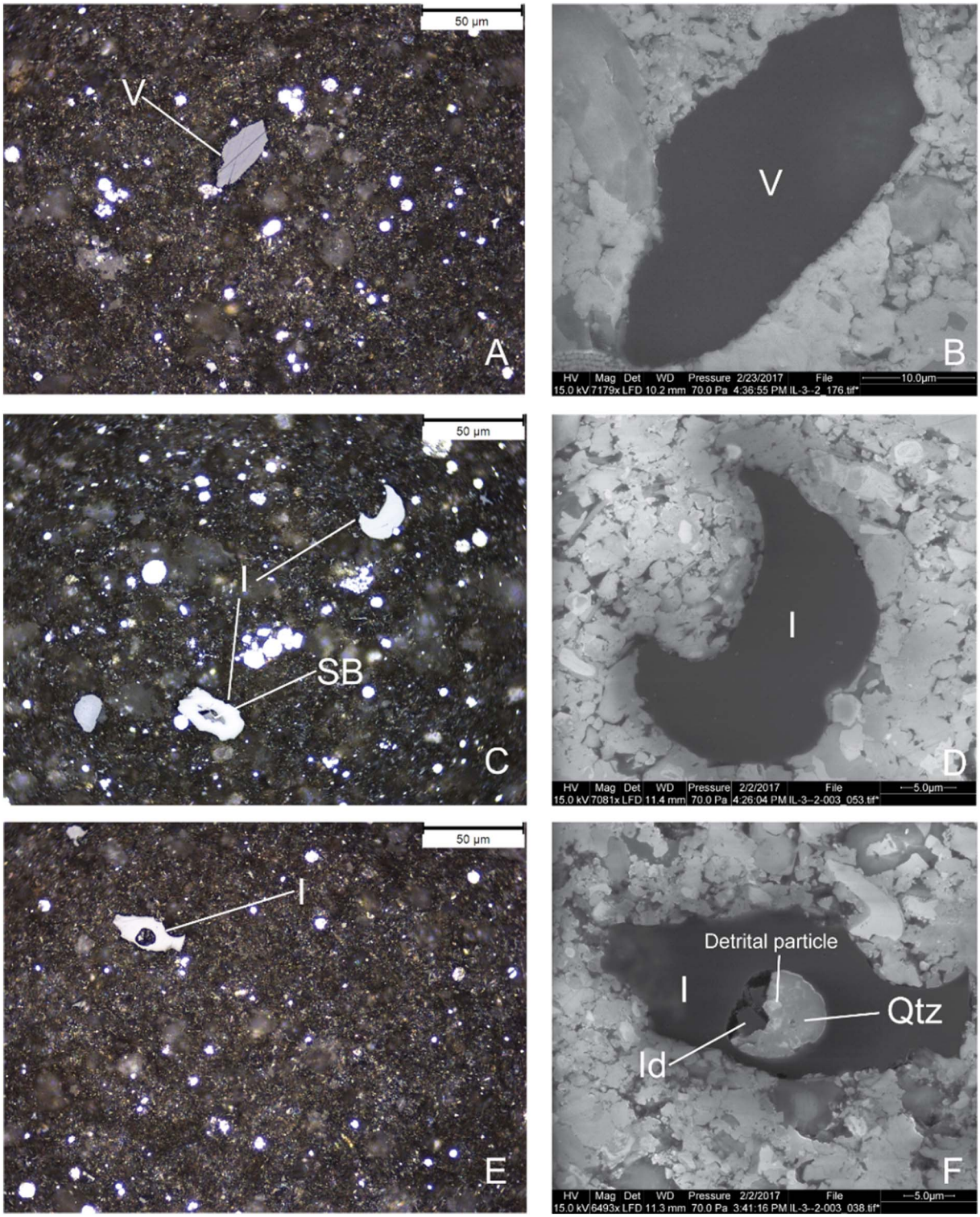

Fig. 7. Photomicrographs of primary organic matter under reflected light and oil immersion (A, C, E), and their correlative SEM images (B, D, F, secondary electron images) in the gas-window-maturity sample, R_o 1.42%. (A) Vitrinite; (B) SEM image of vitrinite in A; (C) Inertinite without cellular pores; (D) SEM image of inertinite in C. (E) Inertinite with cellular pores; (F) SEM image of inertinite in E. The cellular pores are filled with clay-sized detrital particles, authigenic quartz and inertodetrinite. V = vitrinite; I = inertinite; Id = inertodetrinite; SB = solid bitumen; Qtz = quartz.

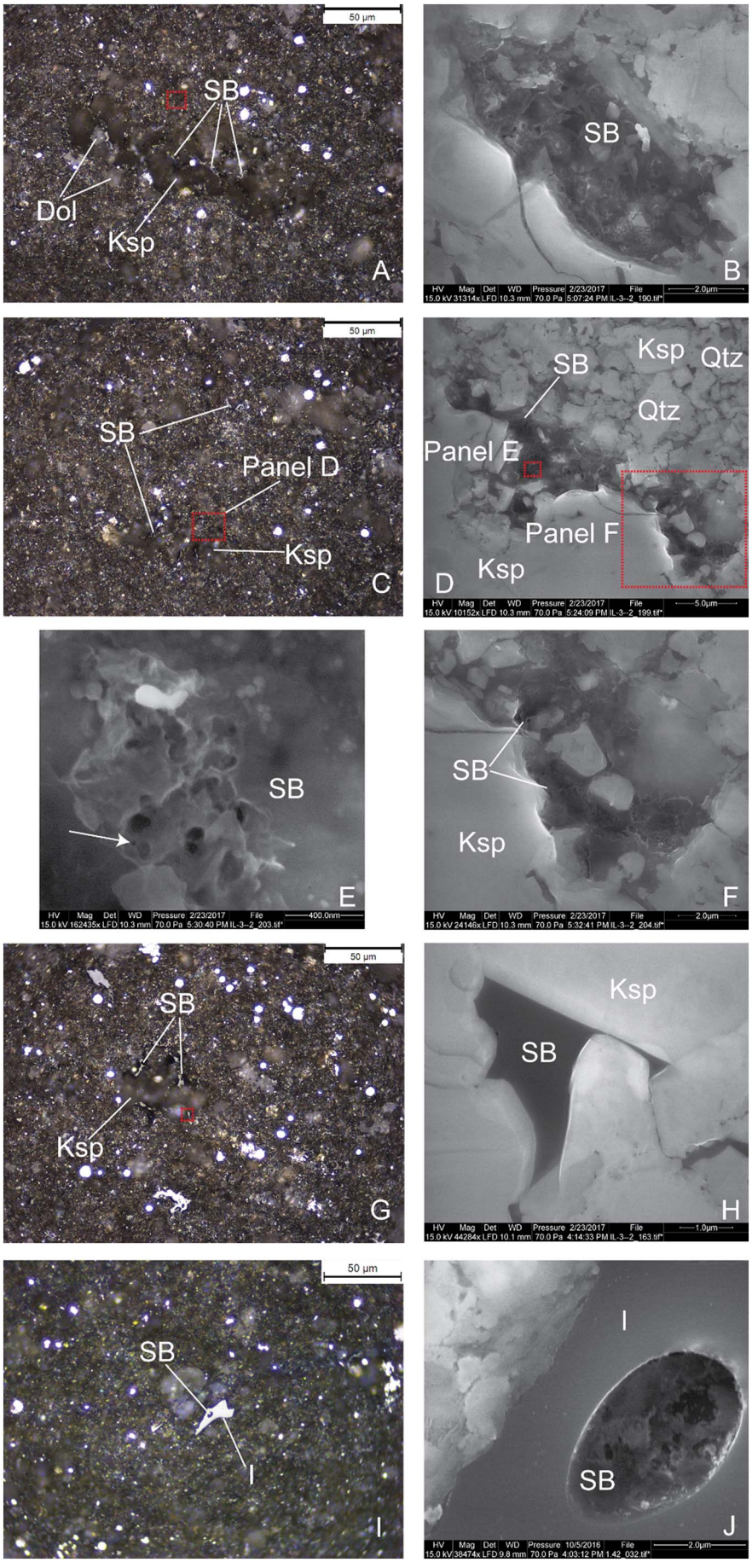

Fig. 8. Photomicrographs of solid bitumen (SB) under reflected light and oil immersion (A, C, G, I), and their correlative SEM images (B, D–F, H, J, secondary electron images) in the gas-window-maturity sample, R_o 1.42%. (A, C, G) SB filling pore space between mineral grains (quartz, dolomite, and K-feldspar); (B) SEM image of the red dotted framed area in A. This SB with secondary nanopores is almost unidentifiable in A; (D–F) SEM images of SB with well-developed secondary nanopores. The smallest visible pore size is 20 nm in diameter (white arrow in E); (H) SEM image of the red dotted framed area in G. This SB shows no SEM-visible pores; (I) SB filling cellular pores in inertinite; (J) SEM image of inertinite and SB in cellular pores. This SB shows secondary nanopores. I = inertinite; SB = solid bitumen; Qtz = quartz; Dol = dolomite; Ksp = K-feldspar.

studied samples, SB was observed from early maturity to gas-window maturity. The transition from AOM to SB (Fig. 4E–F) at a maturity of R_o 0.55% indicates that an SB network followed the original AOM network. Cardott et al. (2015) suggested that a post-oil SB network could have developed along the AOM network. Solid bitumen becomes smaller and more porous during thermal maturation. Porous SB is almost unidentifiable using an optical microscope under reflected light and oil immersion because incident light is mostly absorbed by the pores in SB and is not reflected. Sanei et al. (2015) reported that SB with nanopores could result in a lower reflectance measurement than its true value.

Solid bitumen fills the pore space in shale reservoirs in a similar manner as mineral cement. Camp (2016a) identified bitumen and pyrobitumen "cement" as a void-filling material within matrix pores, microfossil internal voids, and microfractures in the lower Eagle Ford Formation (Late Cretaceous) of south Texas. Cardott et al. (2015) identified speckled, wispy, and connected post-oil SB in the Woodford Shale (Late Devonian-Early Mississippian) of Oklahoma. Mastalerz and Glikson (2000) identified cleat and vein bitumen and cell-filling bitumen in coal. In our study, SB mainly occupies interparticle space (space between quartz, dolomite, K-feldspar, clay, and mica grains) and cavity space (cellular pores in inertinite). Large pieces of SB that occupy interparticle space (~50 μm, Figs. 3I, 4A, E, 6A) might be converted from former oil-prone kerogen particles (AOM or alginite), because pores of that size and shape should have been destroyed by compaction and cementation before the onset of hydrocarbon generation.

Solid bitumen (migrabitumen) that fills pore space between mineral grains is plausibly interconnected three-dimensionally and forms an organic network in tight shale reservoirs. Porosity can be reduced by the filling of pores with bitumen when oil-prone type I/II kerogen is transformed to liquid hydrocarbons (Mastalerz et al., 2013). Wei et al. (2014) studied the pore structure of thermally mature organic-rich shales before and after bitumen extraction and concluded that partial filling of pores with bitumen and oil caused the decrease of microporosity (< 2 nm) and mesoporosity (2–50 nm) of shales at thermal maturities greater than R_o 0.55%.

4.3. Pore development in organic matter during thermal maturation

Cellular pores (0.2–10 μm) in inertinite were observed in each sample. They are typically filled with authigenic quartz (Figs. 3E–F, 5E–F, 7E–F) or SB (Figs. 4C–D, 6G–H, 8I–J). Cellular pores are primary organic pores (Mukhopadhyay, 2015) and are also described as intraparticle OM pores in plant fragments (Canter et al., 2016). Inertinite, oxidized or burned woody materials, has a very low H/C ratio and no potential for hydrocarbon generation and secondary pore development. Loucks et al. (2017) reported that type III kerogen (woody materials) does not develop OM pores during thermal maturation. Since inertinite is discrete OM in the shale matrix, cellular pores in it do not contribute effectively to hydrocarbon migration through a continuous pore network in black shales.

No pores were observed in vitrinite in the New Albany Shale throughout the entire maturity range (Figs. 3B, 5B, 7B). However, well-developed secondary pores in vitrinite that are formed by the expulsion of gaseous hydrocarbons were observed in coal under SEM at a maturity of R_o 0.65 to 0.9% (Zhang et al., 2003). A potential explanation for this difference is that the vitrinite in black shales does not have much hydrocarbon-generating potential because precursor wood fragments experienced some degree of oxidization during transport to the depositional sites. Wei et al. (2016) studied the functional group abundances in various organic macerals in the New Albany Shale using micro-FTIR and concluded that aliphatic functional groups in vitrinite were partially oxidized during transport to the place of deposition.

Alginite does not host organic pores in the early mature sample. The cavity of *Tasmanites* algae is either compacted (Fig. 3E, G) or filled with authigenic minerals such as pyrite (Fig. 3I) or quartz (Schieber, 1996; Schieber et al., 2000; Schieber and Baird, 2001). Schieber (2013) and Löhr et al. (2015) reported that *Tasmanites* cysts are non-porous under SEM in the early mature New Albany Shale and immature Woodford Shale, respectively. However, alginite can develop secondary organic pores during the process of thermal degradation to pre-oil bitumen. The pores in alginite and flow characteristics indicate that some liquid and gaseous hydrocarbons exited the alginite during the degradation process.

Solid-bitumen-hosted pores were not observed in the early mature sample (R_o 0.55%). Hackley et al. (2017) reported that SB does not host organic pores in the immature Green River Shale. Secondary organic pores (20–1000 nm) were observed in SB at the maturity of R_o 0.80% and R_o 1.42% (Figs. 6D–F, 8B, D–F). The nanopores (< 1000 nm) in SB are formed by the generation and expulsion of liquid and gaseous hydrocarbons. In our study, pores in SB are very rare in the oil-window-maturity sample and exist only in small particles of SB, whereas SB that hosts organic pores is very common in the gas-window-maturity sample. Loucks et al. (2017) studied pore types in the lacustrine shale in the Late Triassic Yanchang Formation and concluded that most OM-hosted pores are in migrated SB. Reed et al. (2014) studied organic pores in the oil-window-maturity Barnett Shale (Mississippian) of Texas and suggested that small particles of OM that host pores could be SB. Löhr et al. (2015) reported that smaller OM domains are more porous than large ones in the gas-window-maturity Woodford Shale. The reason for small particles of SB being more porous than large pieces could be that small particles of SB are earlier generations of SB (migrabitumen) that fill small pore spaces between mineral grains, whereas large pieces of SB are newly generated SB from oil-prone kerogen particles and have not experienced advanced thermal maturation. An alternative explanation could be due to the large specific surface area in contact with pore water and surrounding minerals that could catalyze the thermal degradation of OM (Goldstein, 1983; Huizinga et al., 1987; Seewald, 2003). Lu et al. (2015) also reported that OM pores commonly occur along OM-mineral contacts.

Solid bitumen that fills cavities in inertinite appears to be more porous than SB that occupies interparticle space at the same maturity (Figs. 6H, 8J). The SB filling cellular pores might be an earlier generation of SB, because otherwise authigenic mineral cement (e.g., quartz, pyrite or calcite) would fill the cellular pores during diagenesis. Milliken et al. (2014) interpreted homogenous OM that fills a foraminifera test in the Eagle Ford Formation to be secondary OM (SB) at a maturity of R_o 0.5%. Mastalerz and Glikson (2000) reported that SB in inertinite cells is more aromatic (post-gas generation bitumen), and SB occurring in veins and cleats is more aliphatic (pre-gas generation bitumen).

The SB network hosts secondary nanopores formed by thermal degradation and cracking. Cardott et al. (2015) recognized nanopores in post-oil SB networks in the Woodford Shale. Because SB makes up the organic network above the maturity of R_o 0.80% and develops secondary nanopores during thermal maturation, it plays a significant role in hydrocarbon storage and migration. Very rare structured kerogen particles are not transformed to bitumen during thermal maturation and can host organic pores in both oil-window- and gas-window-maturity black shales (e.g., Loucks et al., 2012, Fig. 11A–B; Reed et al., 2014, Fig. 1B), but because of their scarcity, their role in hydrocarbon storage and migration is less important than SB.

We emphasize that the discussion of organic pores in this study relates to pores larger than 20 nm. As such, our observations are limited to larger mesopores and macropores (> 50 nm). Numerous studies using different techniques, such as gas adsorption, neutron scattering, molecular simulation and TEM documented pores smaller than 20 nm in OM (Loucks et al., 2009; Curtis et al., 2011; Mastalerz et al., 2012; Rexer et al., 2014; Bousige et al., 2016). For example, Curtis et al. (2011) reported 3 nm pores in the sponge-like structure of OM in the Barnett Shale using the scanning transmission electron microscopy technique. Mastalerz et al. (2012) studied the pore structure of coal and

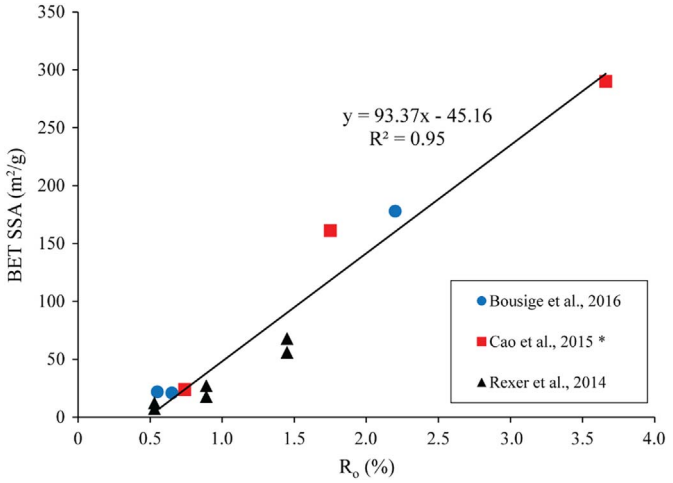

Fig. 9. Relationship between BET specific surface area of extracted organic matter from black shales and vitrinite reflectance (R_o).
*R_o of the samples in Cao et al. (2015) was calculated according to the relationship between T_{max} and R_o from Jarvie et al. (2001): $R_o = 0.018 \times T_{max} - 7.16$.

shale using low-pressure N_2 and CO_2 adsorption and concluded that OM is the main contributor to the micropore network in coal and shale; such small pores are beyond the resolution of SEM.

Organic matter contributes significantly to the methane sorption capacity of gas shales, especially in thermally mature shale gas systems (Zhang et al., 2013). The BET (Brunauer-Emmett-Teller) SSA (specific surface area) of OM in gas shales increases with thermal maturity (Fig. 9; Rexer et al., 2014; Cao et al., 2015; Bousige et al., 2016). The increase of SSA of OM during thermal maturation results from both the increase of microporosity caused by the evolution of macromolecular structure of OM (Bousige et al., 2016) and the development of meso- and macroporosity caused by the generation and expulsion of hydrocarbons (Loucks et al., 2009; Wang and Reed, 2009; Bernard et al., 2012). It has been well documented that micropores in OM macromolecular structure contribute significantly to the sorptive capacity of coal and shale reservoirs (Ambrose et al., 2010; Passey et al., 2012), but larger pores in three-dimensionally interconnected SB are more important in hydrocarbon storage and migration (especially methane storage and migration).

In the USA, the New Albany Shale of the Illinois Basin is time-equivalent with the Ohio Shale of the Appalachian Basin, the Antrim Shale of the Michigan Basin, the Chattanooga Shale of the Black Warrior Basin and the Bakken Shale of the Williston Basin (Schieber, 1998; Strąpoć et al., 2010). The infill of void space by SB that is transformed from oil-prone kerogens can reduce both porosity and permeability of shale reservoirs at peak-oil-window maturity (Mastalerz et al., 2013). However, secondary organic pores developed during thermal maturation can provide space and pathways for oil and gas storage and migration (Wang and Reed, 2009; Passey et al., 2012). To better characterize unconventional reservoirs in shale oil/gas systems, we must understand the contribution of organic pores to porosity, pore size distribution, specific surface area, permeability, and the sorptive capacity of organic-rich shales at different thermal maturities and with varying TOC contents under geological temperature and pressure conditions.

5. Conclusions

A combination of reflected light and SEM microscopy allows us to document the development of meso- and macropores in different types of organic matter with increasing thermal maturity in organic-rich shales, a task that cannot be accomplished using SEM technique alone. Applying these two complementary techniques to a set of Devonian-Mississippian New Albany Shale (kerogen type II sequence) samples leads to the following conclusions:

1) Organic pores in organic-rich shales can be primary or secondary. Primary organic pores are original cellular pores in terrestrial plant fragments. Secondary organic pores are mainly solid-bitumen-hosted and controlled by thermal maturity as well as organic maceral type.
2) Cellular pores (0.2–10 μm) in inertinite are typically filled with authigenic quartz or solid bitumen, and they were observed from early mature to gas-window-maturity samples. Vitrinite and inertinite do not develop secondary organic pores that can be resolved by SEM during thermal maturation. Alginite developed secondary organic pores during the process of transforming to pre-oil bitumen, which indicates that some liquid and gaseous hydrocarbons left the alginite during the degradation process. Pores in organic matter 20 to 1000 nm in diameter are mainly solid-bitumen-hosted in the studied shales, and they are more common in the gas-window-maturity shale than in the oil-window-maturity shale. The solid bitumen network that hosts secondary organic nanopores plays a significant role in hydrocarbon storage and migration.
3) Solid bitumen exists in early mature (R_o 0.55%) to gas-window-maturity (R_o 1.42%) samples and occupies interparticle space (space between quartz, dolomite, K-feldspar, clay, and mica grains) and cavity space (cellular pores in inertinite). A solid bitumen network developed along the original AOM network in these organic-rich shales. Solid bitumen becomes smaller and more porous during thermal maturation, and particles having well-developed secondary nanopores are almost unidentifiable under an optical microscope.
4) Alginite derived from *Tasmanites* cysts matures later than amorphous organic matter. At a maturity of R_o 0.80%, AOM has undergone complete degradation to hydrocarbons and bitumen, whereas alginite was in the process of transforming to pre-oil bitumen. Alginite at R_o 0.80% shows weak orange yellow fluorescence compared to strong greenish-yellow fluorescence in the early mature samples. Solid bitumen became the dominant organic matter when oil-prone kerogens (AOM and alginite) were transformed to hydrocarbons and bitumen, and secondary organic nanopores developed in solid bitumen when oil and gas were generated and expelled. Vitrinite and inertinite derived from terrestrial woody materials do not have high hydrocarbon generation potential and are present as discrete particles across the entire maturity range.

Acknowledgments

This research was supported by the sponsors of the Indiana University Shale Research Consortium, a Geological Society of America Graduate Student Research Grant and an Indiana Geological and Water Survey John Barratt Patton Award. Financial support from the China Scholarship Council is also gratefully acknowledged.

References

Ambrose, R.J., Hartman, R.C., Diaz-Campos, M., Akkutlu, I.Y., Sondergeld, C.H., 2010. New pore-scale considerations for shale gas in place calculations. In: SPE Unconventional Gas Conference. Society of Petroleum Engineers, Pittsburgh, Pennsylvania, USA, pp. 17. SPE 131772. https://doi.org/10.2118/131772-MS.

Beier, J.A., Hayes, J.M., 1989. Geochemical and isotopic evidence for paleoredox conditions during deposition of the Devonian-Mississippian New Albany Shale, southern Indiana. Geol. Soc. Am. Bull. 101 (6), 774–782. http://dx.doi.org/10.1130/0016-7606(1989)101<0774:GAIEFP>2.3.CO;2.

Bernard, S., Wirth, R., Schreiber, A., Schulz, H.-M., Horsfield, B., 2012. Formation of nanoporous pyrobitumen residues during maturation of the Barnett Shale (Fort Worth Basin). Int. J. Coal Geol. 103, 3–11. http://dx.doi.org/10.1016/j.coal.2012.04.010.

Bousige, C., Ghimbeu, C.M., Vix-Guterl, C., Pomerantz, A.E., Suleimenova, A., Vaughan, G., Garbarino, G., Feygenson, M., Wildgruber, C., Ulm, F.-J., Pellenq, R.J.-M., Coasne, B., 2016. Realistic molecular model of kerogen's nanostructure. Nat. Mater. 15 (5), 576–582. http://dx.doi.org/10.1038/NMAT4541.

Camp, W.K., 2016a. Diagenetic evolution of organic matter cements in unconventional shale reservoirs. Houst. Geol. Soc. Bull. 58 (6), 29–31.
Camp, W.K., 2016b. Strategies for identifying organic matter types in SEM. In: AAPG Search and Discovery, (Article No. 90283).
Canter, L., Zhang, S., Sonnenfeld, M., Bugge, C., Guisinger, M., Jones, K., 2016. Primary and secondary organic matter habit in unconventional reservoirs. In: Olson, T. (Ed.), Imaging Unconventional Reservoir Pore Systems. AAPG Memoir 112pp. 9–23. http://dx.doi.org/10.1306/13592014M1123691.
Cao, T., Song, Z., Wang, S., Xia, J., 2015. A comparative study of the specific surface area and pore structure of different shales and their kerogens. Sci. China Earth Sci. 58 (4), 510–522. http://dx.doi.org/10.1007/s11430-014-5021-2.
Cardott, B.J., Landis, C.R., Curtis, M.E., 2015. Post-oil solid bitumen network in the Woodford Shale, USA—a potential primary migration pathway. Int. J. Coal Geol. 139, 106–113. http://dx.doi.org/10.1016/j.coal.2014.08.012.
Chalmers, G.R., Bustin, R.M., Power, I.M., 2012. Characterization of gas shale pore systems by porosimetry, pycnometry, surface area, and field emission scanning electron microscopy/transmission electron microscopy image analyses: examples from the Barnett, Woodford, Haynesville, Marcellus, and Doig units. AAPG Bull. 96 (6), 1099–1119. http://dx.doi.org/10.1306/10171111052.
Chou, M.-I.M., Dickerson, D.R., Chou, S.-F.J., Sargent, M.L., 1991. Hydrocarbon Source Potential and Organic Geochemical Nature of Source Rocks and Crude Oils in the Illinois Basin. Illinois State Geological Survey, Illinois Petroleum 136, Illinois (39 pp.).
Cluff, R.M., 1980. Paleoenvironment of the New Albany Shale Group (Devonian-Mississippian) of Illinois. J. Sediment. Res. 50 (3), 767–780.
Collell, J., Galliero, G., Vermorel, R., Ungerer, P., Yiannourakou, M., Montel, F., Pujol, M., 2015. Transport of multicomponent hydrocarbon mixtures in shale organic matter by molecular simulations. J. Phys. Chem. C 119 (39), 22587–22595. http://dx.doi.org/10.1021/acs.jpcc.5b07242.
Curiale, J.A., 1986. Origin of solid bitumens, with emphasis on biological marker results. Org. Geochem. 10 (1–3), 559–580. http://dx.doi.org/10.1016/0146-6380(86)90054-9.
Curtis, M.E., Ambrose, R.J., Sondergeld, C.H., Rai, C.S., 2011. Transmission and scanning electron microscopy investigation of pore connectivity of gas shales on the nanoscale. In: North American Unconventional Gas Conference and Exhibition. Society of Petroleum Engineers, The Woodlands, Texas, USA, pp. 10. SPE 144391. https://doi.org/10.2118/144391-MS.
Curtis, M.E., Cardott, B.J., Sondergeld, C.H., Rai, C.S., 2012. Development of organic porosity in the Woodford Shale with increasing thermal maturity. Int. J. Coal Geol. 103, 26–31. http://dx.doi.org/10.1016/j.coal.2012.08.004.
Fan, E., Tang, S., Zhang, C., Guo, Q., Sun, C., 2014. Methane sorption capacity of organics and clays in high-over matured shale-gas systems. Energy Explor. Exploit. 32 (6), 927–942. http://dx.doi.org/10.1260/0144-5987.32.6.927.
Fishman, N.S., Hackley, P.C., Lowers, H.A., Hill, R.J., Egenhoff, S.O., Eberl, D.D., Blum, A.E., 2012. The nature of porosity in organic-rich mudstones of the Upper Jurassic Kimmeridge Clay Formation, North Sea, offshore United Kingdom. Int. J. Coal Geol. 103, 32–50. http://dx.doi.org/10.1016/j.coal.2012.07.012.
Ganser, M., Weiss, A., 2008. Reflected-light microscope. U.S. Patent No. 7,379,238.
Goldstein, T.P., 1983. Geocatalytic reactions in formation and maturation of petroleum. AAPG Bull. 67 (1), 152–159.
Hackley, P.C., Cardott, B.J., 2016. Application of organic petrography in North American shale petroleum systems: a review. Int. J. Coal Geol. 163, 8–51. http://dx.doi.org/10.1016/j.coal.2016.06.010.
Hackley, P.C., Valentine, B.J., Voortman, L.M., Van Oosten Slingeland, D.S.B., Hatcherian, J., 2017. Utilization of integrated correlative light and electron microscopy (iCLEM) for imaging sedimentary organic matter. J. Microsc. 267 (3), 371–383. http://dx.doi.org/10.1111/jmi.12576.
Hao, F., Zou, H., Lu, Y., 2013. Mechanisms of shale gas storage: Implications for shale gas exploration in China. AAPG Bull. 97 (8), 1325–1346. http://dx.doi.org/10.1306/02141312091.
Huizinga, B.J., Tannenbaum, E., Kaplan, I.R., 1987. The role of minerals in the thermal alteration of organic matter—III. Generation of bitumen in laboratory experiments. Org. Geochem. 11 (6), 591–604. http://dx.doi.org/10.1016/0146-6380(87)90012-X.
International Committee for Coal Petrology (ICCP), 1998. The new vitrinite classification (ICCP System 1994). Fuel 77 (5), 349–358. http://dx.doi.org/10.1016/S0016-2361(98)80024-0.
International Committee for Coal Petrology (ICCP), 2001. The new inertinite classification (ICCP System 1994). Fuel 80, 459–471. http://dx.doi.org/10.1016/S0016-2361(00)00102-2.
Jacob, H., 1989. Classification, structure, genesis and practical importance of natural solid oil bitumen ("migrabitumen"). Int. J. Coal Geol. 11 (1), 65–79. http://dx.doi.org/10.1016/0166-5162(89)90113-4.
Jarvie, D.M., Claxton, B.L., Henk, F., Breyer, J.T., 2001. Oil and shale gas from the Barnett Shale, Fort. Worth Basin, Texas. In: AAPG Annual Meeting Program. vol. 10. pp. A100.
Jarvie, D.M., Hill, R.J., Ruble, T.E., Pollastro, R.M., 2007. Unconventional shale-gas systems: the Mississippian Barnett Shale of north-central Texas as one model for thermogenic shale-gas assessment. AAPG Bull. 91 (4), 475–499. http://dx.doi.org/10.1306/12190606068.
Lazar, O.R., 2007. Redefinition of the New Albany Shale of the Illinois Basin: An Integrated, Stratigraphic, Sedimentologic, and Geochemical Study. Ph.D. dissertation. Indiana University, Bloomington (336 pp.).
Lineback, J.A., 1964. Stratigraphy and depositional environment of the New Albany Shale (Upper Devonian and Lower Mississippian) in Indiana. Ph.D. dissertation. Indiana University (136 pp.).
Lineback, J.A., 1968. Subdivisions and depositional environments of New Albany Shale (Devonian-Mississippian) in Indiana. AAPG Bull. 52 (7), 1291–1303.
Löhr, S.C., Baruch, E.T., Hall, P.A., Kennedy, M.J., 2015. Is organic pore development in gas shales influenced by the primary porosity and structure of thermally immature organic matter. Org. Geochem. 87, 119 − 132. http://dx.doi.org/10.1016/j.orggeochem.2015.07.010.
Loucks, R.G., Reed, R.M., 2014. Scanning-electron-microscope petrographic evidence for distinguishing organic-matter pores associated with depositional organic matter versus migrated organic matter in mudrocks. Gulf Coast Assoc. Geol. Soc. J. 3, 51–60.
Loucks, R.G., Reed, R.M., Ruppel, S.C., Jarvie, D.M., 2009. Morphology, genesis, and distribution of nanometer-scale pores in siliceous mudstones of the Mississippian Barnett Shale. J. Sediment. Res. 79 (12), 848–861. http://dx.doi.org/10.2110/jsr.2009.092.
Loucks, R.G., Reed, R.M., Ruppel, S.C., Hammes, U., 2012. Spectrum of pore types and networks in mudrocks and a descriptive classification for matrix-related mudrock pores. AAPG Bull. 96 (6), 1071 − 1098. http://dx.doi.org/10.1306/08171111061.
Loucks, R.G., Ruppel, S.C., Wang, X., Ko, L., Peng, S., Zhang, T., Rowe, H.D., Smith, P., 2017. Pore types, pore-network analysis, and pore quantification of the lacustrine shale-hydrocarbon system in the Late Triassic Yanchang Formation in the southeastern Ordos Basin, China. Interpretation 5 (2), SF63–SF79. http://dx.doi.org/10.1190/INT-2016-0094.1.
Lu, J., Ruppel, S.C., Rowe, H.D., 2015. Organic matter pores and oil generation in the Tuscaloosa marine shale. AAPG Bull. 99 (2), 333–357. http://dx.doi.org/10.1306/08201414055.
Mastalerz, M., Glikson, M., 2000. In-situ analysis of solid bitumen in coal: examples from the Bowen Basin and the Illinois Basin. Int. J. Coal Geol. 42 (2), 207 − 220. http://dx.doi.org/10.1016/S0166-5162(99)00040-3.
Mastalerz, M., He, L., Melnichenko, Y.B., Rupp, J.A., 2012. Porosity of coal and shale: insights from gas adsorption and SANS/USANS techniques. Energy Fuel 26 (8), 5109–5120. http://dx.doi.org/10.1021/ef300735t.
Mastalerz, M., Schimmelmann, A., Drobniak, A., Chen, Y., 2013. Porosity of Devonian and Mississippian New Albany Shale across a maturation gradient: insights from organic petrology, gas adsorption, and mercury intrusion. AAPG Bull. 97 (10), 1621–1643. http://dx.doi.org/10.1306/04011312194.
Milliken, K.L., Rudnicki, M., Awwiller, D.N., Zhang, T., 2013. Organic matter–hosted pore system, Marcellus formation (Devonian), Pennsylvania. AAPG Bull. 97 (2), 177–200. http://dx.doi.org/10.1306/07231212048.
Milliken, K.L., Ko, L.T., Pommer, M., Marsaglia, K.M., 2014. SEM petrography of Eastern Mediterranean sapropels: Analogue data for assessing organic matter in oil and gas shales. J. Sediment. Res. 84 (11), 961–974. http://dx.doi.org/10.2110/jsr.2014.75.
Misch, D., Mendez-Martin, F., Hawranek, G., Onuk, P., Gross, D., Sachsenhofer, R.F., 2016. SEM and FIB-SEM investigations on potential gas shales in the Dniepr-Donets Basin (Ukraine): pore space evolution in organic matter during thermal maturation. In: IOP Conference Series: Materials Science and Engineering. 109, Paper No.: 012010, http://dx.doi.org/10.1088/1757-899X/109/1/012010.
Mukhopadhyay, P.K., 2015. Primary or secondary organic pore network and parallel adsorption sites in shale: Dependency on organic facies and maturity in selected Canadian source rocks. In: AAPG Search and Discovery Article No. 80472.
Passey, Q.R., Bohacs, K.M., Esch, W.L., Klimentidis, R., Sinha, S., 2010. From oil-prone source rock to gas-producing shale reservoir-geologic and petrophysical characterization of unconventional shale-gas reservoirs. In: International Oil and Gas Conference and Exhibition in China. Society of Petroleum Engineers, Beijing, China, pp. 29. SPE 131350. https://doi.org/10.2118/131350-MS.
Passey, Q.R., Bohacs, K.M., Esch, W.L., Klimentidis, R., Sinha, S., 2012. My source rock is now my reservoir-Geologic and petrophysical characterization of shale-gas reservoirs. In: AAPG Search and Discovery Article No. 80231.
Pickel, W., Kus, J., Flores, D., Kalaitzidis, S., Christanis, K., Cardott, B.J., Misz-Kennan, M., Rodrigues, S., Hentschel, A., Hamor-Vido, M., Crosdale, P., Wagner, N., ICCP, 2017. Classification of liptinite–ICCP System 1994. Int. J. Coal Geol. 169, 40–61. http://dx.doi.org/10.1016/j.coal.2016.11.004.
Reed, R.M., Loucks, R.G., Ruppel, S.C., 2014. Comment on "Formation of nanoporous pyrobitumen residues during maturation of the Barnett Shale (Fort Worth Basin)" by Bernard et al. (2012). Int. J. Coal Geol. 127, 111–113. http://dx.doi.org/10.1016/j.coal.2013.11.012.
Rexer, T.F., Mathia, E.J., Aplin, A.C., Thomas, K.M., 2014. High-pressure methane adsorption and characterization of pores in Posidonia shales and isolated kerogens. Energy Fuel 28 (5), 2886–2901. http://dx.doi.org/10.1021/ef402466m.
Ripley, E.M., Shaffer, N.R., Gilstrap, M.S., 1990. Distribution and geochemical characteristics of metal enrichment in the New Albany Shale (Devonian-Mississippian), Indiana. Econ. Geol. 85 (8), 1790–1807. http://dx.doi.org/10.2113/gsecongeo.85.8.1790.
Ross, D.J.K., Bustin, R.M., 2009. The importance of shale composition and pore structure upon gas storage potential of shale gas reservoirs. Mar. Pet. Geol. 26 (6), 916–927. http://dx.doi.org/10.1016/j.marpetgeo.2008.06.004.
Sanei, H., Haeri-Ardakani, O., Wood, J.M., Curtis, M.E., 2015. Effects of nanoporosity and surface imperfections on solid bitumen reflectance (BRo) measurements in unconventional reservoirs. Int. J. Coal Geol. 138, 95–102. http://dx.doi.org/10.1016/j.coal.2014.12.011.
Schieber, J., 1996. Early diagenetic silica deposition in algal cysts and spores: a source of sand in black shales? J. Sediment. Res. 66, 175–183. http://dx.doi.org/10.1306/D42682ED-2B26-11D7-8648000102C1865D.
Schieber, J., 1998. Developing a sequence stratigraphic framework for the Late Devonian Chattanooga Shale of the southeastern USA: Relevance for the Bakken Shale. In: Eighth International Williston Basin Symposium. Saskatchewan Geological Society Special Publication 13, pp. 58–68.
Schieber, J., 2010. Common themes in the formation and preservation of intrinsic porosity in shales and mudstones-illustrated with examples across the Phanerozoic. In:

SPE Unconventional Gas Conference. Society of Petroleum Engineers, Pittsburgh, Pennsylvania, USA, pp. 10. SPE 132370. https://doi.org/10.2118/132370-MS.
Schieber, J., 2013. SEM observations on ion-milled samples of Devonian black shales from Indiana and New York: the petrographic context of multiple pore types. In: Camp, W., Diaz, E., Wawak, B. (Eds.), Electron Microscopy of Shale Hydrocarbon Reservoirs. AAPG Memoir Vol. 102pp. 153–171. http://dx.doi.org/10.1306/13391711M1023589.
Schieber, J., Baird, G., 2001. On the origin and significance of pyrite spheres in Devonian black shales of North America. J. Sediment. Res. 71 (1), 155–166. http://dx.doi.org/10.1306/051600710155.
Schieber, J., Krinsley, D., Riciputi, L., 2000. Diagenetic origin of quartz silt in mudstones and implications for silica cycling. Nature 406 (6799), 981–985. http://dx.doi.org/10.1038/35023143.
Schieber, J., Lazar, R., Bohacs, K., Klimentidis, R., Dumitrescu, M., Ottmann, J., 2016. An SEM study of porosity in the Eagle Ford Shale of Texas—Pore types and porosity distribution in a depositional and sequence-stratigraphic Context. In: Breyer, J.A. (Ed.), The Eagle Ford Shale: A Renaissance in U.S. Oil Production. AAPG Memoir 110pp. 167–186. http://dx.doi.org/10.1306/13541961M1103589.
Seewald, J.S., 2003. Organic–inorganic interactions in petroleum-producing sedimentary basins. Nature 426 (6964), 327–333. http://dx.doi.org/10.1038/nature02132.
Slatt, R.M., O'Brien, N.R., 2011. Pore types in the Barnett and Woodford gas shales: Contribution to understanding gas storage and migration pathways in fine-grained rocks. AAPG Bull. 95 (12), 2017–2030. http://dx.doi.org/10.1306/03301110145.
Sondergeld, C.H., Ambrose, R.J., Rai, C.S., Moncrieff, J., 2010. Micro-structural studies of gas shales. In: SPE Unconventional Gas Conference. Society of Petroleum Engineers, Pittsburgh, Pennsylvania, USA, pp. 17. SPE 131771. https://doi.org/10.2118/131771-MS.
Strąpoć, D., Mastalerz, M., Schimmelmann, A., Drobniak, A., Hasenmueller, N.R., 2010. Geochemical constraints on the origin and volume of gas in the New Albany Shale (Devonian–Mississippian), eastern Illinois Basin. AAPG Bull. 94 (11), 1713–1740. http://dx.doi.org/10.1306/06301009197.
Sutton, M.A., Li, N., Joy, D.C., Reynolds, A.P., Li, X., 2007. Scanning electron microscopy for quantitative small and large deformation measurements part I: SEM imaging at magnifications from 200 to 10,000. Exp. Mech. 47 (6), 775–787. http://dx.doi.org/10.1007/s11340-007-9042-z.
Taylor, G.H., Teichmüller, M., Davis, A., Diessel, C.F.K., Littke, R., Robert, P., 1998. Organic Petrology. Gebrüder Borntraeger, Stuttgart, Berlin (704 pp.).
Valentine, B.J., Hackley, P.C., 2016. Bridging the gap between optical and electron microscopy: The importance of correlative microscopy for understanding dispersed organic matter. In: AAPG Search and Discovery Article No. 90283.
Vandenbroucke, M., Largeau, C., 2007. Kerogen origin, evolution and structure. Org. Geochem. 38 (5), 719–833. http://dx.doi.org/10.1016/j.orggeochem.2007.01.001.
Vigran, J.O., Mørk, A., Forsberg, A.W., Weiss, H.M., Weitschat, W., 2008. Tasmanites algae—contributors to the Middle Triassic hydrocarbon source rocks of Svalbard and the Barents Shelf. Polar Research 27 (3), 360–371. http://dx.doi.org/10.1111/j.1751-8369.2008.00084.x.
Wang, F.P., Reed, R.M., 2009. Pore networks and fluid flow in gas shales. In: SPE Annual Technical Conference and Exhibition. Society of Petroleum Engineers, New Orleans, Louisiana, USA, pp. 8. SPE 124253. https://doi.org/10.2118/124253-MS.
Waples, D.W., Marzi, R.W., 1998. The universality of the relationship between vitrinite reflectance and transformation ratio. Org. Geochem. 28 (6), 383–388. http://dx.doi.org/10.1016/S0146-6380(97)00122-8.
Wei, L., Mastalerz, M., Schimmelmann, A., Chen, Y., 2014. Influence of Soxhlet-extractable bitumen and oil on porosity in thermally maturing organic-rich shales. Int. J. Coal Geol. 132, 38–50. http://dx.doi.org/10.1016/j.coal.2014.08.003.
Wei, L., Wang, Y., Mastalerz, M., 2016. Comparative optical properties of macerals and statistical evaluation of mis-identification of vitrinite and solid bitumen from early mature Middle Devonian–Lower Mississippian New Albany Shale: Implications for thermal maturity assessment. Int. J. Coal Geol. 168, 222–236. http://dx.doi.org/10.1016/j.coal.2016.11.003.
Xue, H., Jiang, P., Xu, R., Zhao, B., Zhou, S., 2016. Characterization of the reservoir in Lower Silurian and Lower Cambrian shale of south Sichuan Basin, China. J. Nat. Gas Sci. Eng. 29, 150–159. http://dx.doi.org/10.1016/j.jngse.2015.12.023.
Zhang, H., Li, X., Hao, Q., He, D., Zhuang, J., 2003. Scanning Electron Microscopic Study of Coal in China. Geological Publishing House, Beijing, pp. 70–71 (In Chinese).
Zhang, T., Ellis, G.S., Stephen, C., Milliken, K., Lewan, M., Sun, X., 2013. Effect of organic matter properties, clay mineral type and thermal maturity on gas adsorption in organic-rich shale systems. In: Unconventional Resources Technology Conference. Society of Petroleum Engineers, American Association of Petroleum Geologists, Society of Exploration Geophysicists, Denver, Colorado, USA, pp. 6. SPE 168862. https://doi.org/10.1190/urtec2013-205.
Zuber, M.D., Williamson, J.R., Hill, D.G., Sawyer, W.K., Frantz Jr., J.H., 2002. A comprehensive reservoir evaluation of a shale reservoir-the New Albany shale. In: SPE Annual Technical Conference and Exhibition. Society of Petroleum Engineers, San Antonio, Texas, USA, pp. 12. SPE 77469. https://doi.org/10.2118/77469-MS.